Signatures of electron correlations in the transport properties of quantum dots

Kristian Jauregui* and Wolfgang Häusler
I. Institut für Theoretische Physik, Jungiusstrasse 9, 20355 Hamburg, Federal Republic of Germany

Dietmar Weinmann
Centre d'Etudes Nucléares Saclay, Service de Physique de l'État Condensé, F-91191 Gif-sur-Yvette Cedex, France

Bernhard Kramer
I. Institut für Theoretische Physik, Jungiusstrasse 9, 20355 Hamburg, Federal Republic of Germany

(Received 22 September 1995)

The transition matrix elements between the correlated N and $N+1$ electron states of a quantum dot are calculated by numerical diagonalization. They are the central ingredient for the linear and nonlinear transport properties, which we compute using a rate equation. The experimentally observed variations in the heights of the linear conductance peaks can be explained. The knowledge of the matrix elements as well as the stationary populations of the states allows us to assign the features observed in the nonlinear transport spectroscopy to certain transitions and contains valuable information about the correlated electron states.

By using modern nanostructure fabrication technology a few electrons can be confined to very small regions in space.[1] In these so-called quantum dots or artificial atoms the Coulomb interaction between the electrons is very important for understanding their quantum-mechanical properties. Weak coupling to external reservoirs via tunnel barriers allows us to observe single-electron transport effects like the Coulomb blockade oscillations in the linear conductance at milli-Kelvin temperatures.[2–4] In nonlinear transport, features are observed that are closely related to the excitation spectrum of the interacting electrons.[5]

Transport involves transitions between the many-body eigenstates of the confined electrons. They are approximated as products of one-particle states within the charging model where the Coulomb interaction is modeled phenomenologically by the capacity of the quantum dot.[6] This is not sufficient to explain, e.g., the experimentally observed negative differential conductances.[7] Especially at low electron densities, correlations between the electrons are crucial. This was explicitly shown for a quasi-one-dimensional (1D) box[8] where the correlation leads to N pronounced peaks in the charge-density distribution if the mean electron distance r_s exceeds the effective Bohr radius a_B^* with $a_B^* \equiv (m_e/m)\varepsilon a_B$ (ε is the relative dielectric constant; m is the effective mass). In the present paper we use the same model to investigate the influence of the spatial properties of the correlated many-electron states on the linear and nonlinear transport properties of an artificial atom. An investigation in a similar spirit was recently performed for a harmonic confining potential in two dimensions.[9] However, transport properties were not calculated and only the transition between $N=2$ and 3 electron states was studied in this work. We demonstrate here that the current-voltage characteristics obtained by solving a stationary master equation exhibits very specific signatures of the electron correlations. They influence the transition matrix elements and also stationary occupation probabilities of the states. Some of the "lines" observed in nonlinear transport spectra are even enhanced. Such a result cannot be obtained by considering only the transition rates.

We will show that, apart from the restrictions due to spin selection rules discussed earlier,[10,11] transitions are suppressed or enhanced when taking into account the spatial properties of the wave functions. The heights of the peaks in the linear conductance become nonequal even without taking into account the energy dependence of tunneling matrix elements. In nonlinear transport the excited levels of the quantum dot that *can* be observed are closely related to the *most prominent allowed transitions* and to the *highest stationary occupation probabilities*.

As a model for the quantum dot we consider a quasi-1D square well[8,12] of length $L=9.5a_B^*$ and $N\leqslant 4$. The corresponding mean electron density is close to the one in experiments on GaAs-Al_xGa_{1-x}As heterostructures where the mean distance between the electrons is about $3a_B^*$ (≈ 10 nm).[2,4,5]

Including the spin degree of freedom σ, the dot Hamiltonian reads

$$H_D=\sum_{n,\sigma}(\epsilon_n-e\phi)c^\dagger_{n,\sigma}c_{n,\sigma} + \sum_{\substack{n_1\cdots n_4\\ \sigma,\sigma'}} V_{n_4n_3n_2n_1}c^\dagger_{n_4\sigma}c^\dagger_{n_3\sigma'}c_{n_2\sigma'}c_{n_1\sigma}. \quad (1)$$

The electrostatic potential ϕ depends on the gate and transport (bias) voltages that are applied to the system and shifts the energies of the one-electron levels. $V_{n_4n_3n_2n_1}$ is the matrix element of the interaction $V(x,x')=e^2/\varepsilon\sqrt{(x-x')^2+\lambda^2}$. The cutoff at short distances simulates a small transversal spread of the wave functions ($\lambda \ll L$) and provides finite $V_{n_4n_3n_2n_1}$.

In the limit of high tunnel barriers, transport is determined by the eigenstates of the isolated dot. From the latter we

TABLE I. Sequence of increasing energy eigenvalues E_α^S together with their total spins S.

$N=2$	$N=3$	$N=4$
$E_0^0,\ E_1^1$	$E_0^{1/2},\ E_1^{1/2},\ E_2^{3/2}$	$E_0^0,E_1^1,E_2^1,E_3^0,E_4^1,E_5^2$

calculate the transition probabilities between N and $(N\pm1)$ electron states. Each energy eigenstate is simultaneously an eigenstate of the total spin $\hat{S}^2=(\hat{\sigma}_1+\cdots+\hat{\sigma}_N)^2$, which implies a $(2S+1)$-fold degeneracy with respect to $\hat{S}_z$ in the absence of a magnetic field.

We include $n=1,\ldots,M$ one-electron states $\varphi_n(x)\chi_\sigma$ when diagonalizing H_D. Here, φ_n is a spatial one-electron function and χ_σ a spinor with $\sigma=\downarrow,\uparrow$. The Hamiltonian matrix in the basis of Slater determinants is of the rank of the binomial number $r=C_{2M}^N$ ($r<1.5\times10^4$, for $M=10,\ldots,13$). The Lanczos method was used when $r>3\times10^3$.

By its algorithm[13] the Lanczos diagonalization provides only one eigenvector $|\Psi^S\rangle_{\rm Lanc}$ for each energy eigenvalue. The calculation of transition rates is considerably facilitated when using eigenstates of $\hat{S}_z$. Usually $|\Psi^S\rangle_{\rm Lanc}$ is a linear combination of all of the $2S+1$ vectors in the subspace of Zeeman levels. In order to recover the eigenvectors of $\hat{S}_z$ we apply projectors $\hat{P}_{S_z}|\Psi^S\rangle_{\rm Lanc}\propto|\Psi^{S,S_z}\rangle$ corresponding to a specific S_z. After normalization $|\Psi^{S,S_z}\rangle \equiv\Sigma_{\nu=1}^r b_\nu^{S,S_z}|\nu\rangle$ can be expanded into the Slater determinants $|\nu\rangle=c^\dagger_{n_1\sigma_1}\cdots c^\dagger_{n_N\sigma_N}|0\rangle$ of the noninteracting electrons. The coefficients b_ν^{S,S_z} are obtained after diagonalization, projection, and renormalization. By construction we have $b_\nu^{S,S_z}=0$ if $\sigma_1+\cdots+\sigma_N\neq S_z$. The method would fail in the unlikely case that $|\Psi^S\rangle_{\rm Lanc}$ is accidentally perpendicular (within the numerical accuracy) to one of the $|\Psi^{S,S_z}\rangle$. The procedure can also be applied to higher-dimensional models.

To study transport properties, we use the tunneling Hamiltonian and the usual rate equation approach.[10,11] Then the dc current through the quantum dot,

$$I\equiv I^{L/R}=(-/+)e\sum_{i,j(j\neq i)}P_i\Gamma_{i,j}^{L/R}(N_j-N_i), \tag{2}$$

corresponds to the rate of electron passages through the left or the right barrier. I is computed from the stationary occupation probabilities P_j, which are solutions of the equation $\Sigma_{j(j\neq i)}(\Gamma_{i,j}P_j-\Gamma_{j,i}P_i)=0$. The transition rates between all of the many-electron states indexed by j are $\Gamma_{j,i}=\Gamma_{j,i}^L+\Gamma_{j,i}^R$.

TABLE II. Comparison between numerically calculated matrix elements $M_{j,i}$, Eq. (4), and corresponding values obtained by neglecting the spatial part of the wave function, $C_{j,i}$, Eq. (5), for the nonvanishing transition probabilities $|\Psi^S_{i(N=2)}\rangle\rightarrow|\Psi^{S\pm1/2}_{j(N=3)}\rangle$.

$\langle\Psi^{S\pm1/2}_{j(N=3)}\|$	$c^\dagger$	$\|\Psi^S_{i(N=2)}\rangle$	$M_{j,i}$	$C_{j,i}$
$\langle\Psi_0^{1/2}\|$	$c^\dagger$	$\|\Psi_0^0\rangle$	0.85	1
$\langle\Psi_1^{1/2}\|$	$c^\dagger$	$\|\Psi_0^0\rangle$	0.04	
$\langle\Psi_0^{1/2}\|$	$c^\dagger$	$\|\Psi_1^1\rangle$	0.32	1/3
$\langle\Psi_1^{1/2}\|$	$c^\dagger$	$\|\Psi_1^1\rangle$	0.29	
$\langle\Psi_2^{3/2}\|$	$c^\dagger$	$\|\Psi_1^1\rangle$	0.43	2/3

TABLE III. Same as Table II for transitions $|\Psi^S_{i(N=3)}\rangle\rightarrow|\Psi^{S\pm1/2}_{j(N=4)}\rangle$. Different columns are used for state with same spins S but different energies (see Table I).

$\langle\Psi^S_{j(N=4)}\|$	$c^\dagger$	$\|\Psi^S_{i(N=3)}\rangle$	$M_{j,i}$	$C_{j,i}$
$\langle\Psi_0^0\|$	$c^\dagger$	$[\|\Psi_0^{1/2}\rangle;\|\Psi_1^{1/2}\rangle]$	[0.37 ; 0.15]	1/4
$\langle\Psi_3^0\|$	$c^\dagger$	$[\|\Psi_0^{1/2}\rangle;\|\Psi_1^{1/2}\rangle]$	[0.01 ; 0.10]	
$\langle\Psi_1^1\|$	$c^\dagger$	$[\|\Psi_0^{1/2}\rangle;\|\Psi_1^{1/2}\rangle]$	[0.37 ; 0.11]	
$\langle\Psi_2^1\|$	$c^\dagger$	$[\|\Psi_0^{1/2}\rangle;\|\Psi_1^{1/2}\rangle]$	[0.03 ; 0.49]	3/4
$\langle\Psi_4^1\|$	$c^\dagger$	$[\|\Psi_0^{1/2}\rangle;\|\Psi_1^{1/2}\rangle]$	[0.00 ; 0.16]	
$\langle\Psi_1^1\|$	$c^\dagger$	$\|\Psi_2^{3/2}\rangle$	0.28	
$\langle\Psi_2^1\|$	$c^\dagger$	$\|\Psi_2^{3/2}\rangle$	0.23	3/8
$\langle\Psi_4^1\|$	$c^\dagger$	$\|\Psi_2^{3/2}\rangle$	0.15	
$\langle\Psi_5^2\|$	$c^\dagger$	$\|\Psi_3^{3/2}\rangle$	0.41	5/8

Time-dependent perturbation theory yields

$$\Gamma_{j,i}^{L/R}=t^{L/R}\left|\sum_{n,\sigma}\langle\Psi_j|c^\dagger_{n,\sigma}|\Psi_i\rangle\right|^2 f^{L/R}(E) + t^{L/R}\left|\sum_{n,\sigma}\langle\Psi_i|c_{n,\sigma}|\Psi_j\rangle\right|^2[1-f^{L/R}(-E)], \tag{3}$$

for transition probabilities between the eigenstates $|\Psi_i\rangle$ and $|\Psi_j\rangle$ of H_D with $N_j=N_i+1$ in lowest order in the tunneling. The indices i and j contain, in particular, the electron number N, the total spin S, and S_z. $t^{L/R}$ are the tunneling rates through the left/right barrier. The electron has to provide the energy difference $E=E_j-E_i$ when entering or leaving the dot. The Fermi-Dirac distribution functions $f^{L/R}(E)$ describe the left/right reservoirs with chemical potentials $\mu^{L/R}$.

The energy spectrum of the N electrons for the densities studied consists of multiplets.[8,12] The energy differences Ω between the latter are considerably larger than the intramultiplet energy differences Δ. They are important only for large transport voltages. For a GaAs-Al_xGa_{1-x}As heterostructure of length $L=9.5a_B^*$ with $N=4$, $\Omega\approx6.2$ meV, and $\Delta\approx62$ μeV. For small transport voltages we can restrict ourselves to transitions between states within the lowest multiplets (Table I). The total number of states within the multiplets, including the S_z degeneracy, is 2^N.

In the following we discuss the influence of the correlations between the electrons on the total transition probability,

$$M_{j,i}=\frac{1}{2}\,\frac{1}{2S_i+1}\sum_{S_{zi}=-S_i}^{S_i}\ \sum_{S_{zj}=-S_j}^{S_j}\left|\sum_{n,\sigma}\langle\Psi_j|c^\dagger_{n,\sigma}|\Psi_i\rangle\right|^2, \tag{4}$$

where the spins S_{zi} and S_{zj} refer to the states $|\Psi_i\rangle$ and $\langle\Psi_j|$, respectively. The matrix elements $\langle\Psi_j|c^\dagger_{n,\sigma}|\Psi_i\rangle$ imply first of all a spin selection rule; namely, that each added or removed electron can change both the total spin S and the

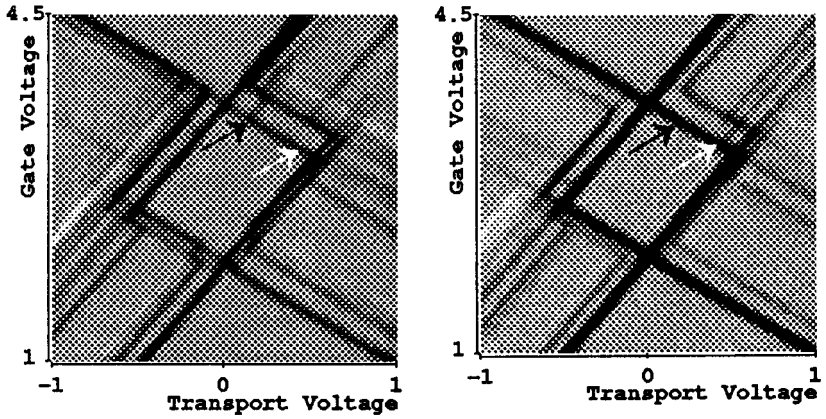

FIG. 1. Differential conductance versus transport and gate voltages (in units of e/a_B^*) in linear gray scale (dark: positive; bright: negative). The electron number inside the diamond-shaped Coulomb blockade region is $N=3$. Left: transition probabilities proportional to $C_{j,i}$. Right: transition probabilities proportional to $M_{j,i}$. The arrows are explained in the text.

magnetic quantum number S_z only by $\pm 1/2$. In Refs. 10 and 11 these selection rules were included via the Clebsch-Gordan coefficients. They describe the combination of the initial spin state (S_i, S_{zi}) with an electron $(1/2, \pm 1/2)$ to form the final state (S_j, S_{zj}) and yield

$$C_{j,i}=\frac{S_i+1}{2S_i+1}\,\delta_{S_j,S_i+1/2}+\frac{S_i}{2S_i+1}\,\delta_{S_j,S_i-1/2} \tag{5}$$

after summation over S_{zi} and S_{zj}. This approach ignores the spatial degrees of freedom which make the $M_{j,i}$ considerably different from the $C_{j,i}$.

In Tables II and III the numerically calculated $M_{j,i}$ and the corresponding $C_{j,i}$ are shown for transitions between two and three and three and four electrons in the dot, respectively. The truncation of the Hilbert space to $M \leqslant 13$ leads to an absolute error of 10^{-3} (Table II) or 10^{-2} (Table III). In a few cases we checked the improvement achieved by using $M=14$ single-electron levels.

Some transitions are almost completely suppressed in the case of the $M_{j,i}$ compared to the $C_{j,i}$. The two reasons can be seen from

$$\left|\sum_{n,\sigma}\langle\Psi_j|c^\dagger_{n,\sigma}|\Psi_i\rangle\right|^2=\left|\sum_{\nu_i,\nu_j} b_{\nu_i} b_{\nu_j}\sum_{n,\sigma}\langle\nu_j|c^\dagger_{n,\sigma}|\nu_i\rangle\right|^2. \tag{6}$$

TABLE IV. The four largest expansion coefficients $b_\nu^{\{N,E_i^S,S_z\}}$ of $|\Psi_0^{1/2}\rangle$ and $|\Psi_3^0\rangle$ needed to calculate the entry 0.01 in Table III. The basis states $|\nu\rangle$ are illustrated for $N=3$, 4 according to the occupations of single-electron levels. Only two transitions between these states are possible by creating or annihilating one electron, marked with $*$ or with ‡.

$b_\nu^{\{3,E_0^{1/2},-1/2\}}$	-0.64	$+0.39^*$	-0.32	$-0.29^‡$
Electronic distribution	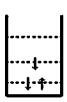	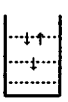	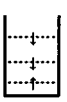	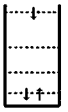
Electronic distribution	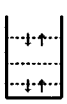	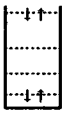	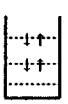	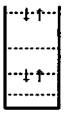
$b_\nu^{\{4,E_3^0,0\}}$	-0.37	$+0.35^‡$	$+0.33^*$	-0.25

Firstly, it may be impossible to create $\langle\nu_j|$ by adding one electron to $|\nu_i\rangle$ (spatial selection rule) for the largest $|b_{\nu_i}b_{\nu_j}|$. Secondly, the various contributions to the summation over ν_i and ν_j may cancel due to different signs of $b_{\nu_i}b_{\nu_j}$. This latter cancellation seems to have been neglected, in Ref. 9. As an example, Table IV shows the four main contributions for the $|\Psi_0^{1/2}\rangle$ for $N=3$ and $|\Psi_3^0\rangle$ for $N=4$, together with their corresponding electronic configurations (see Table I for the notation). They are needed to calculate $M_{3,0}$ in Table III. Of the 16 possible transitions shown in Table IV, only two (marked with $*$ and ‡) fulfill the spatial selection rule. In addition, their contribution to $M_{3,0}$ cancel each other due to opposite signs $[M_{3,0}\approx(-0.35\times 0.29+0.33\times 0.39)^2=0.0006]$. This explains the smallness of the corresponding transition probability. Another example is the transition between the first excited state for $N=3$ and the ground state for $N=2$, $\langle\Psi_1^{S'=1/2}|c^\dagger|\Psi_0^{S=0}\rangle$, Table II. In this case, we were able to follow the evolution of the many-electron states down to zero interaction, ending at Slater determinants $|\nu_i\rangle$ and $|\nu_j\rangle$, between which the spatial selection rule forbids transitions.

The effect on *nonlinear transport properties* is demonstrated in Fig. 1. It shows gray-scale plots of the differential conductance versus the gate voltage V_G and the transport voltage. In Fig. 1 (left) the $\Gamma_{j,i}^{L/R}$ were assumed to be proportional to $C_{j,i}$ (Ref. 10) while the calculated $M_{j,i}$ [Eq. (3)] were used in Fig. 1 (right). Gray areas correspond to regions of zero differential conductance. Black and white lines are

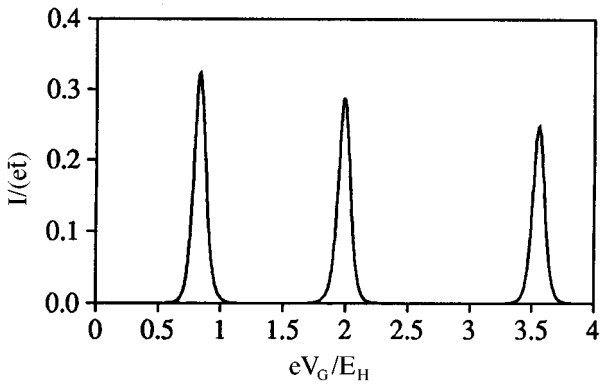

FIG. 2. Current versus gate voltage for small transport voltage ($V<\Delta$) using Eq. (3). Temperature is 10 mK. The first peak corresponds to oscillations between $N=1$ and 2 electrons.

related to positive and negative differential conductances, respectively (spin blockade[10,11]). They reflect excited many-electron states that become available for transport when gate and/or bias voltages are increased. On average, the number of lines is reduced in Fig. 1 (right) as compared to Fig. 1 (left) (e.g., black arrows). This reflects the suppression of transition matrix elements by the spatial selection rule discussed above. In some regions, however, the differential conductance is even enhanced (cf. white arrows in Fig. 1). This is caused by considerable upheavals in the stationary occupation probabilities P_j obtained from the rate equation when the full matrix elements are considered in (3).

The conductance peaks at low transport voltages shows different peak heights, as presented in Fig. 2. This is directly related to the spatial properties of the many-body states. Other works[14,15] explain this feature, also observed experimentally,[3,5] within the framework of noninteracting electrons pictured by semiclassical chaotic motions. The question of how far this picture can be generalized to the correlated electron situation deserves further research. Similar results in the presence of magnetic fields were shown in Ref. 16.

In summary, we have studied the electron transport through a quantum dot taking fully into account the correlated eigenstates of the interacting electrons inside the dot. The spatial selection rule is shown to explain the suppression of certain transitions between N and $(N\pm 1)$ electron states that would be allowed when taking into account only the spin selection rules. Despite the obtained tendency towards reduced transition probabilities $M_{j,i}$, some of the peaks in the differential conductance are even enhanced as a result of considerable changes in the stationary occupation probabilities. Furthermore, the correlations between the electrons induced by the Coulomb interaction lead to characteristic variations in the heights of the linear conductance peaks. Our results show that nonlinear transport spectroscopy provides, in principle, valuable information about the correlated dot states. To extract this information, and the corresponding physics, however, very careful theoretical modeling is required.

This work was supported by grants of the Deutsche Forschungsgemeinschaft and the EEC (Contracts Nos. SCC*-CT90-0020 and CHRX-CT930126).

*Electronic address: jauregui@physnet.uni-hamburg.de

[1] M. A. Kastner, Rev. Mod. Phys. **64**, 849 (1992).
[2] U. Meirav, M. A. Kastner, and S. J. Wind, Phys. Rev. Lett. **65**, 771 (1990); L. P. Kouwenhoven *et al.*, in *Single Charge Tunneling*, edited by H. Grabert [Z. Phys. B **85**, 367 (1991)].
[3] A. T. Johnson *et al.*, Phys. Rev. Lett. **69**, 1592 (1992).
[4] P. L. McEuen *et al.*, Physica B **189**, 70 (1993).
[5] J. Weis, R. Haug, K. v. Klitzing, and K. Ploog, Phys. Rev. Lett. **71**, 4019 (1993).
[6] L. P. Kouwenhoven *et al.*, in *Single Charge Tunneling*, edited by H. Grabert [Z. Phys. B **85**, 317 (1991)].
[7] W. Pfaff, D. Weinmann, W. Häusler, B. Kramer, and U. Weiss, Z. Phys. B **96**, 201 (1994).
[8] K. Jauregui, W. Häusler, and B. Kramer, Europhys. Lett. **24**, 581 (1993).
[9] D. Pfannkuche and S. E. Ulloa, Phys. Rev. Lett. **74**, 1194 (1995).
[10] D. Weinmann, W. Häusler, W. Pfaff, B. Kramer, and U. Weiss, Europhys. Lett. **26**, 467 (1994).
[11] D. Weinmann, W. Häusler, and B. Kramer, Phys. Rev. Lett. **74**, 984 (1995).
[12] W. Häusler and B. Kramer, Phys. Rev. B **47**, 435 (1993).
[13] J. K. Cullum and R. A. Willoughby, *Lanczos Algorithms for Large Symmetric Eigenvalue Computations* (Birkhäuser, Boston, 1985), Vol. I.
[14] A. D. Stone and H. Bruus, Physica B **189**, 43 (1993).
[15] V. I. Fal'ko and K. B. Efetov, Phys. Rev. B **50**, 11 267 (1994).
[16] J. J. Palacios, L. Martin-Moreno, and C. Tejedor, Europhys. Lett. **23**, 495 (1993).